Environmental Science & Technology

Article

Cite This: Environ. Sci. Technol. XXXX, XXX, XXX−XXX

pubs.acs.org/est

Short-Term Impacts of the Aliso Canyon Natural Gas Blowout on Weather, Climate, Air Quality, and Health in California and Los Angeles

Mark Z. Jacobson*,†

†Department of Civil and Environmental Engineering, Stanford University, Stanford, California 94305, United States

ABSTRACT: The Aliso Canyon (Porter Ranch), California, natural gas blowout lasted 112 days, from October 23, 2015 to February 11, 2016, releasing 97 100 metric tonnes of methane, 7300 tonnes of ethane, and a host of other hydrocarbons into the Southern California air. This study estimates the impacts of the leak on transient weather, climate, air quality, and health in California and the Los Angeles Basin using a nested global-through-local weather−climate−air quality computer model. Results suggest that the Aliso Canyon leak may have increased the mixing ratios of multiple emitted hydrocarbon gases throughout California. Subsequent gas-phase photochemistry increased the mixing ratios of additional byproducts, including carbon monoxide, formaldehyde, acetaldehyde, peroxyacetyl nitrate, and ozone. Increases in air temperatures aloft and lesser increases at the surface due to thermal-infrared radiation absorption by methane stabilized the air over much of California, slightly reducing clouds, precipitation, and near-surface wind speed with greater reductions in Los Angeles than in California. The reduction in precipitation, in particular, increased $PM_{2.5}$ concentration, with a greater increase in Los Angeles than in California. The higher $PM_{2.5}$ increased estimated premature mortality in California by +32 (9−54) to +43 (15−66), depending on the set of relative risks used. Despite higher $PM_{2.5}$ in Los Angeles due to the leak, premature mortalities there were more ambiguous, ranging from a mean decrease of −7 to a mean increase of +15, for 2 simulations with different resolution and boundary conditions. The remaining mortalities occurred in the Central Valley and San Francisco Bay Area. Ozone premature mortalities away from the leak increased by <1. The study did not evaluate potential health impacts, including cancers, immediately near the leak. As such, the Aliso Canyon leak affected temperatures, pollution, and health throughout California. Future leaks will also likely have impacts.

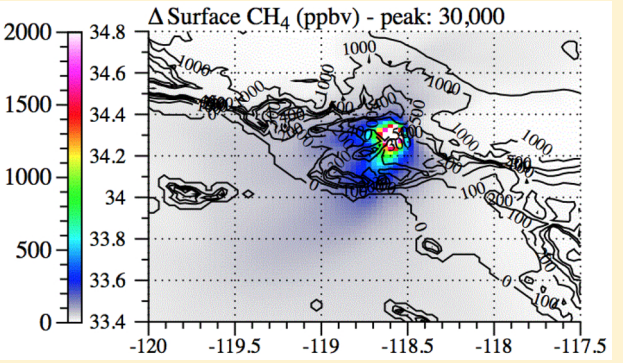

1. INTRODUCTION

This study examines the health and short-term local climate and air quality impacts of the Aliso Canyon, CA (34.315 N, 118.564167 W) natural gas leak. The blowout was from well SS-25, one of 115 wells tapping the Aliso Canyon natural gas storage facility owned by Southern California Gas Company, a subsidiary of Sempra Energy. Most of the leak occurred between October 23, 2015 and February 11, 2016 (112 days), resulting in the emissions of ∼97 000 metric tonnes of methane, ∼7300 tonnes of ethane, and quantities of several other hydrocarbons.[1−4] For annual emissions in the South Coast Air Basin of methane and ethane have been reported as ∼413 000 and 23 000 tonnes per year, respectively.[5] This corresponds to about 127 000 tonnes of methane and 7000 tonnes of ethane emitted in California from non-leak sources during the Aliso Canyon leak period. Thus, the leak effectively doubled the background emission rate of methane and ethane during the period of the leak.

The 5 billion cubic feet (bcf) of gas lost to the air during the Aliso Canyon blowout pales in comparison with the trillion cubic feet of gas lost per year in the United States from venting and blowouts from the 1920s until at least the 1950s.[6] However, Aliso Canyon was the largest single-source U.S. gas leak since the Wheeler County, Texas blowout of October 4, 1981, which lasted 16 months and vented 14.4 bcf of gas to the air.[6]

The Aliso Canyon leak resulted in the evacuation of thousands of nearby residents, sickened hundreds, and caused a loss of energy reserves for building heat and electricity. The cost of the leak as of August 2018 was estimated at over $1 billion.[7]

However, emissions from the leak also spread throughout and outside of California, including to the populated Los Angeles Basin, Central Valley, and San Francisco Bay Area. The modeled impacts of the leak on short-term climate and health in California have not been investigated to date. Such impacts are examined here with the Gas, Aerosol, Transport, Radiation, General Circulation, Mesoscale, and Ocean Model (GATOR-GCMOM), which is a global-through-urban nested climate-weather-air pollution model.[8−21] The model has been

Received: March 10, 2019
Accepted: April 29, 2019
Published: April 29, 2019

DOI: 10.1021/acs.est.9b01495
Environ. Sci. Technol. XXXX, XXX, XXX−XXX

Table 1. Resolutions of the Nested Domains Treated

domain	South−North resolution	West−East resolution	no. of South−North cells	no. of West−East cells	center of Southernmost cell	center of Westernmost cell	no. of layers
global[a]	4°	5°	44	72	86 S	180 W	68
California	0.20°	0.15°	60	95	30 N	129 W	55
Los Angeles	0.018 180 7°	0.030 414°	146	156	32.452 789 N	120.730 939 W	55

[a]The S−N (south-north) resolution of the global domain is 6° for the southernmost and northernmost rows of grid cells, but the centers are considered to be 86 S and 86 N, respectively (thus the next centers are 82 S and 82 N, respectively). For the California simulations, only the Global and California domains are used. For the Los Angeles simulations, all three domains are used.

used and compared with data previously to simulate air pollution in California, Los Angeles, the Central Valley, and the San Francisco Bay Area;[8,9,13,17,21] greenhouse gas plumes in Los Angeles;[13] the impacts of the Fukushima Daichii nuclear accident point source plume on human health in California;[22] and the impacts of urbanization on short-term climate, weather, and pollution.[20,21] Model predictions have been compared with data in 20 peer-reviewed studies, and the model has taken part in 11 multimodel intercomparisons. Additional comparisons with data are shown here. In this study, GATOR-GCMOM is applied to examine the impacts of the Aliso Canyon blowout throughout California at medium resolution and in the Los Angeles Basin at higher resolution, predominantly during the period of the leak.

2. DESCRIPTION OF GATOR-GCMOM

GATOR-GCMOM simulates feedbacks among gas, aerosol, radiative, meteorological, cloud, ocean, lake, sea ice, snow, soil, road, roof, and vegetation processes. It does not include data assimilation or nudging to ensure the model remains purely prognostic. If the model included assimilation or nudging, separating the impacts of such assimilation or nudging from those of model physical, chemical, and dynamic processes would not be possible when quantifying the effects of a perturbation, such as the Aliso gas leak. Below, the model is briefly described. The only update to the model compared with ref 21 was to add the time-dependent emissions from the Aliso Canyon leak.

Meteorological, Transport, Gas, and Surface Processes. In each model domain, from the global to Los Angeles scale, the model solved atmospheric meteorology, atmospheric gas and aerosol transport, ocean circulation, ocean chemistry, and land surface processes as given in ref 21. Gas physical and chemical processes included emissions, photochemistry, gas-to-particle conversion, gas-to-cloud conversion, gas−cloud exchange, gas−ocean exchange, advection, convection, molecular diffusion, turbulent diffusion, and dry deposition. Gas photochemistry was solved with SMVGEAR II for 161 gases and 404 tropospheric and stratospheric kinetic, heterogeneous, and photolysis reactions.

Aerosol Processes. Aerosol processes included anthropogenic and natural emissions, binary and ternary homogeneous nucleation, condensation, dissolution, internal-particle chemical equilibrium, aerosol−aerosol coagulation, aerosol-hydrometeor coagulation, sedimentation, dry deposition, and transport,[10,11,14,21] The model treated any number of discrete aerosol size distributions, each with any number of size bins and chemicals per bin. For this study, one aerosol size distribution with 14 size bins ranging from 2 nm to 50 μm in diameter was used in each grid cell of each domain. Aerosol components in each size bin included black carbon (BC), tar balls, other primary organic carbon, secondary organic carbon, H_2O(aq), H_2SO_4(aq), HSO_4^-, SO_4^{2-}, NO_3^-, Cl^-, H^+, NH_4^+, Na^+, soil dust, pollen, spores, and bacteria.

Convective Cloud, Stratiform Cloud, Aerosol-Cloud Processes. For each simulation, either two or three nested domains were used (Table 1). For the coarser global and California domains, convective clouds were treated at the subgrid scale (with multiple subgrid clouds per column), and stratus clouds are treated at the grid scale. Size- and composition-resolved aerosols and gases were transported vertically within each sub-grid cloud. Size- and composition-resolved cloud and precipitation particles then formed on top of the aerosol size distributions through multiple microphysical processes.[11,14,17]

For the finer-resolved Los Angeles domain, all cloud thermodynamics and microphysics were treated explicitly at the grid scale.[17] Size- and composition-resolved cloud and precipitation particles formed from size- and composition-resolved aerosol particles, and the cloud particles and their components were transported along with gases both horizontally and vertically. In other words, clouds formed and evolved in three dimensions in the innermost domain. On all scales, the model treated three hydrometeor size distributions (liquid, ice, and graupel), each with 30 size bins (0.5 μm to 8 mm in diameter) and tracked concentrations of all aerosol component inclusions in each size bin of each hydrometeor distribution.[11,17]

Radiative Processes. For radiative calculations, each atmospheric model column was divided into clear- and cloudy-sky columns, and separate calculations were performed for each. A two-stream radiative code[23] was used to solve the atmospheric radiative transfer equation for radiances, irradiances, photosynthetically active radiation (PAR), actinic fluxes, and atmospheric heating rates through each model layer in each column, over each of 694 wavelengths amd probability intervals in the ultraviolet, visible, solar-infrared, and thermal-infrared spectra (170 nm to 1000 μm), accounting for gas and size- and composition-dependent aerosol and cloud optical properties.[14,21]

The model accounted for atmospheric scattering and absorption by gases and size- and composition-resolved aerosol and hydrometeor particles. Because the model treated the time-dependent evolution of the size and composition of aerosol particles and clouds and the feedbacks of aerosol particles to atmospheric stability and winds, it accounted for the first indirect effect, second indirect effect, and the semidirect effect of aerosol particles on clouds.[14]

Aerosol and cloud optical properties were calculated by integrating spectral optical properties over all size bins of each aerosol and hydrometeor particle size distribution. Aerosol spectral optical properties of a given size were determined by assuming that black carbon, if present, was a core surrounded

DOI: 10.1021/acs.est.9b01495
Environ. Sci. Technol. XXXX, XXX, XXX−XXX

by a mixed shell and that the aerosol liquid water content is a function of the ambient relative humidity and aerosol composition. Spectral scattering and absorption properties of aerosol particles within clouds but between cloud particles were determined when the aerosol liquid water content was at the relative humidity of the cloud.[14] Cloud drop, ice crystal, and graupel optical properties were determined while accounting for the time-dependent evolution of black carbon, brown carbon, and soil dust within clouds. These three cloud particle inclusions all absorb solar radiation. As such, the model accounted for cloud absorption effects I and II, which are the heating of a cloud due to solar radiation absorption by inclusions within cloud drops and by swollen aerosol particles interstitially between cloud drops, respectively.[14]

Emissions. The time-dependent point-source emission rate of methane from Aliso Canyon (at 34.315°N, 118.564167°W) has been estimated by Conley et al.[1] for days 1−40 (October 23−December 1, 2015) to be an average (range) of ∼53.5 (46.9−60.4) metric tonnes of CH_4 per hour). For days 41−112 (December 2, 2015 to February 11, 2016), the emission rate decreased (Figure 2 and Table S2 in ref 1]. A polynomial that approximately fits the trend for days 41−112 is:

$$\begin{aligned}&\text{tonnes of } CH_4 \text{ per hour}\\ &= 55.962 + x(-2.4128 + x(0.083927\\ &\quad + x(-0.0018108 + x(2.0799 \times 10^{-5} - 9.3676\\ &\quad \times 10^{-8}x))))\end{aligned} \quad (1)$$

where x is the day past start − 40. This polynomial gives emission rates of 53.63, 38.61, 29.8, 24.79, 21.5, 19.51, 18.91, and 19.13 tonnes of CH_4 per hour on days 41, 50, 60, 70, 80, 90, 100, and 112, respectively. It is further assumed here that for days 113−119 (February 12−18, 2016), methane emissions decreased down to a residual of 1 tonne of CH_4 per hour [Table S2 of Conley et al.[1]]. Thereafter, emissions were assumed to be zero. The aggregate methane emissions from the leak between October 23, 2015 and February 11, 2015 from the fit above are 97 127 tonnes of CH_4. Through February 19, 2015, the emissions are 97 295 tonnes of CH_4.

Based on measurements, Conley et al.[1] further estimated the time-dependent emission rates of a variety of other hydrocarbons from the leak (Table 2). Such emissions are treated here by scaling the time-dependent molar methane emissions from the leak by the molar ratio provided in Table 2 of each hydrocarbon to methane.

For this study, pairs of simulations are performed, one with and one without emissions from the leak. In both simulations for each pair, background anthropogenic and natural emissions are included. For the global domain in all simulations, the anthropogenic emission inventory used is the Fifth Assessment Report (AR5) inventory for 2005, assuming the Representative Concentration Pathway (RCP) 4.5 trajectory.[24] This inventory is at 0.5° horizontal resolution. Emitted pollutants include CO, CH_4, acids, alcohols, benzene, butanes, chlorinated hydrocarbons, esters, ethane, ethene, ethers, ethyne, formaldehyde, hexanes, and higher alkanes, ketones, other volatile organic compounds (VOCs), other alkanals, other alkenes, other aromatics, pentanes, propane, propene, terpenes, toluene, trimethylbenzenes, xylene, NO, NO_2, NH_3, SO_2, SO_3, BC, and primary organic carbon (POC). For CO_2, N_2O, CFCs, and HFCs, the EDGAR 2005 inventory is used.[25] Emissions of all components from open biomass and biofuel burning are described in ref 15 as are heat and moisture fluxes from fossil fuel, biomass, and biofuel combustion. Natural emissions from lightning (NO, NO_2, HONO, HNO_3, N_2O, H_2O_2, HO_2, and CO), soils (dust, bacteria, NO, N_2O, H_2, CH_4, H_2S, dimethylsulfide or DMS, OCS, and CS), oceans (bacteria, sea spray, DMS, N_2O, H_2, CH_4, and CH_3Cl), and vegetation (pollen, spores, isoprene, monoterpenes, methanol, and other VOCs) are calculated as a function of modeled meteorology as in ref 18. Jacobson et al. discuss the CO_2 sources and sinks in the model.[20]

For the California and Los Angeles domains (Table 1), the anthropogenic emission inventory used was the 2008 U.S. National Emission Inventory (NEI).[26] The NEI was used because it provides background emissions, not only for California, but also for surrounding states that are part of the California and global model domains. From the point, on-road mobile, non-road mobile, and area source raw emission data, diurnally varying gridded inventories were prepared at the horizontal resolution of each model domain. Table 3 lists the emitted chemicals from the inventory and their annual average emission rates for each domain. The main chemicals relevant to forming ozone are nitrogen oxides and organic gases. The main chemicals relevant to forming $PM_{2.5}$ are directly emitted

Table 2. Emission Rates during the Aliso Canyon Episode (October 23, 2015 to February 11, 2016, or 112 days, Not Including the Residual From February 12−18, 2016, Quantified in the Text) of Different Hydrocarbons from the Aliso Canyon Natural Gas Leak[a]

chemical	molecular weight (g/mol)	mole fraction of CH_4 emissions	episode-emission rate (tonnes of chemical per episode)
methane (CH_4)	16.042	1.0	97,100
ethane (C_2H_6)	30.069	4.01×10^{-2}	7,300
propane (C_3H_8)	44.096	2.23×10^{-3}	595
n-butane (C_4H_{10})	58.122	1.68×10^{-4}	59.1
i-butane (C_4H_{10})	58.122	1.51×10^{-4}	53.1
n-pentane (C_5H_{12})	72.149	3.18×10^{-5}	13.9
i-pentane (C_6H_{12})	72.149	4.75×10^{-5}	20.7
cyclopentane (C_5H_{10})	70.133	3.20×10^{-6}	1.36
n-hexane (C_6H_{14})	86.175	8.11×10^{-6}	4.23
2,3-dimethylbutane (C_6H_{14})	86.175	2.20×10^{-6}	1.15
2-methylpentane (C_6H_{14})	86.175	1.01×10^{-5}	5.27
3-methylpentane (C_6H_{14})	86.175	5.91×10^{-6}	3.08
methylcyclopentane (C_6H_{12})	84.159	9.32×10^{-6}	4.75
cyclohexane (C_6H_{12})	84.159	9.64×10^{-6}	4.91
n-heptane (C_7H_{16})	100.202	4.28×10^{-6}	2.60
n-octane (C_8H_{18})	114.229	1.91×10^{-6}	1.32
n-nonane (C_9H_{20})	128.255	1.15×10^{-6}	0.89
n-decane ($C_{10}H_{22}$)	142.282	7.19×10^{-7}	0.62
benzene (C_6H_6)	78.112	5.15×10^{-6}	2.43
toluene (C_7H_8)	92.138	6.40×10^{-6}	3.57
ethylbenzene (C_8H_{10})	106.165	7.03×10^{-7}	0.45
o,m,p-xylene (C_8H_{10})	106.165	4.52×10^{-6}	2.90

[a]Also shown are the emission rates expressed as a mole fraction of methane's molar emissions, taken from Table S1 of ref 1, except that for ethane, the mole fraction is derived from the reported 7300 metric tonnes of ethane emitted on p 1319. Eq 1 gives the time-dependent mass emission rate of methane used here.

DOI: 10.1021/acs.est.9b01495
Environ. Sci. Technol. XXXX, XXX, XXX−XXX

Table 3. Background (Without the Aliso Canyon Leak) Anthropogenic (Point, On-Road Mobile, Non-Road Mobile, and Area Source) Emission Rates of Gases and Particles in the California and Los Angeles Domains, Defined in Table 1, from the 2008 U.S. National Emissions Inventory (NEI).[26a]

	California domain (includes Nevada)			Los Angeles domain		
species	NEI (Gg/year)	biomass plus biofuel (Gg/year)	biogenic (Gg/year)	NEI (Gg/year)	biomass plus biofuel (Gg/year)	biogenic plus other natural (Gg/year)[b]
carbon monoxide	3715	798		1506	310	
carbon dioxide	337 000	7130		125 000	8548	
nitrogen oxides as NO_2	1048	139	42.9	459	74.5	6.36
organic gases						
methane	301	44.5	307	76.0	20.0	44.1
ethane	22.0	11.4		5.6	5.6	
propane	10.5	4.45		3.56	2.21	
paraffin bond group	366	21.5	231	142	10.2	24.9
ethene	33.7	24.0		13.3	11.8	
propene	6.70	10.8		2.60	5.30	
1,3-butadiene	7.18	3.11		3.20	1.24	
olefin bond group	11.9	11.9	25.2	4.37	5.85	2.72
methanol	1.65	13.3	280	0.56	5.54	30.7
ethanol	12.7	3.52		4.45	1.85	
formaldehyde	9.13	4.31		3.80	1.46	
acetaldehyde	3.00	11.3		1.21	5.50	
higher aldehydes	24.3	20.3		9.51	7.44	
formic acid	0.46	16.5		0.14	7.66	
acetic acid	0.81	22.3		0.25	10.1	
acetone	4.73	1.45		1.55	0.26	
benzene	13.8	15.0		5.04	7.70	
toluene bond group	73.5	6.87		31.8	3.41	
xylene bond group	86.6	2.98		35.5	1.51	
isoprene bond group	0.72	3.52	314	0.26	1.43	74.9
monoterpenes			374			32.1
total organic gas	**990**	**253**	**1531**	**344**	**116**	**209**
sulfur oxides as SO_2	48.2	89.4		16.9	51.1	
ammonia	326	4.23		69.1	1.11	
			$PM_{2.5}$			
organic matter	56.2	101		24.9	36.8	
black carbon	34.5	6.92		15.1	2.58	
sulfate	5.02	1.52		1.93	0.55	
nitrate	0.41	0.78		0.14	0.29	
other	161	3.43		42.5	1.19	
total $PM_{2.5}$	**257**	**114**		**84.6**	**41.4**	
			PM_{10}			
organic matter	117	126	176	47.8	45.8	30.8
black carbon	43.4	8.62		18.8	3.21	
sulfate	8.06	1.89		3.13	0.68	
nitrate	1.33	0.97		0.46	0.36	
other	849	4.27		255	1.48	
soil dust			492			1260
sea spray			3765			225
pollen, spores, and bacteria			1909			157
total PM_{10}	**1019**	**142**	**6342**	**325**	**51.6**	**1673**

[a]Also shown are biomass plus biofuel burning emission rates, described in ref 15 and biogenic and other natural emission rates, calculated during the simulation from current weather data, as in ref 18. [b]Other: road dust, ammonium, sodium, chloride, and metals. Natural aerosol particulate matter is organic carbon from ocean sea spray.

particles and some precursor gases (high-molecular-weight organic gases, sulfur oxides, ammonia, and nitrogen oxides).

Biomass burning, biofuel burning, and natural emissions in the California and Los Angeles domains are calculated with the same methodologies as in the global domain. In comparison with the work of Wunch et al.,[5] who estimate 413 and 23 Gg-C_2H_6/year in 2016, the anthropogenic plus natural methane and ethane emissions from the Los Angeles domain in Table 1 (140 and 11.2 Gg-C_2H_6/year) are very low. The emissions used in the model are the sum of anthropogenic emissions from the 2008 NEI, anthropogenic biomass and biofuel burning emissions, and natural biogenic emission. Part of the reason for the difference is that the model some 2008 NEI emissions, whereas Wunch et al. values were from 2016.

DOI: 10.1021/acs.est.9b01495
Environ. Sci. Technol. XXXX, XXX, XXX−XXX

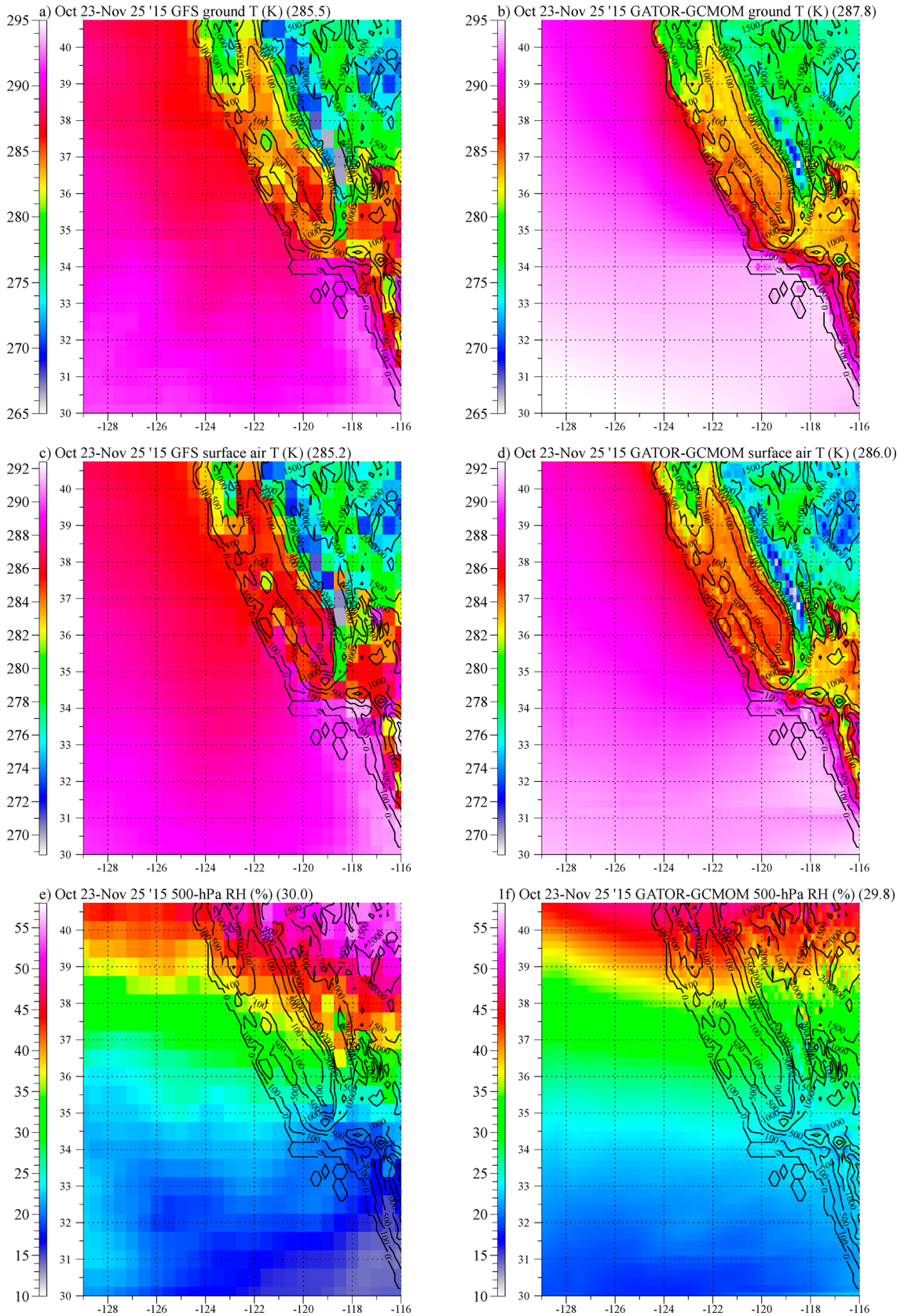

Figure 1. Comparison of modeled parameters over the California domain (defined in Table 1) with GFS[27] reanalysis data for the first month of simulation (October 23, 2015 at 6 GMT to November 25, 2015 at 6 GMT). The GFS fields (at 0.5° resolution) were obtained by averaging GFS files four times per day (00, 06, 12, and 18 GMT) during the period of interest except that data for October 23 at 12 GMT through October 25 at 0 GMT were missing. Numbers in parentheses are domain-averaged values. RH is relative humidity. T is temperature.

DOI: 10.1021/acs.est.9b01495
Environ. Sci. Technol. XXXX, XXX, XXX−XXX

Table 4. Modeled Domain- and Simulation-Averaged Baseline Values (No Leak) and Difference Values (Leak Minus No Leak) For the California and Los Angeles Simulations[a]

species	California no leak	California leak minus no leak (percent change)	Los Angeles no leak	Los Angeles leak minus no leak (percent change)
15 m wind speed (m/s)	5.63	−0.007	4.90	−0.021
38 m wind speed (m/s)	6.29	−0.0057	5.51	−0.012
100 m wind speed (m/s)	7.12	−0.002	6.11	−0.0024
soil moisture (m^3/m^3) (land only)	0.219	−0.20	0.124	+0.52
ground temp. (K)	285.3	+0.0004	285.8	−0.001
15 m air temp. (K)	283.2	+0.0002	284.5	−0.0005
38 m air temp. (K)	283.3	+0.0004	284.6	−0.0004
surface TKE (m^2/s^2)	0.255	−0.005	0.334	+0.025
surface relative humidity (%)	69.6	−0.011	57.8	−0.015
latent heat flux (W/m^2) (+ is up)	86.0	−0.0093	75.3	−0.0050
Sensible heat flux (W/m^2) (+ is up)	15.7	+0.0024	13.8	−0.009
surface TIR irrad (W/m^2) (+ down)	−100.0	−0.031	−107.8	+0.023
surface solar irrad (W/m^2) (+ down)	120.7	+0.029	125.1	−0.0034
surf down−up Sol plus TIR (W/m^2) (+ down)	20.7	+0.043	17.3	−0.17
surface UV irradiance (W/m^2)	5.37	+0.0015	5.49	+0.0016
TOA TIR irrad (W/m^2) (+ down)	−241	+0.005	−247.4	+0.01
TOA solar irrad (W/m^2) (+ down)	166	+0.021	171.4	−0.0062
TOA down−up Sol plus TIR(W/m^2) (+ down)	−74.5	−0.031	−76.0	+0.046
650 nm cloud optical depth	5.92	−0.27	4.02	−0.40
cloud absorption optical depth	0.00015	−0.34	0.00012	−0.42
cloud liquid mass (kg/m^2)	0.021	−0.027	0.017	−1.09
cloud ice mass (kg/m^2)	0.014	+0.053	0.011	−0.49
cloud fraction	0.36	−0.028	0.20	−0.29
precipitation (mm/day)	1.49	−0.037	1.23	−0.19
surface CH_4 (ppbv)	1,846	+0.11	1,842	+0.80
surface C_2H_6 (ppbv)	1.33	+6.3	1.37	+43.3
surface C_4H_6 (ppbv)	0.011	+0.31	0.035	+0.042
surface C_6H_6 (ppbv)	0.18	+0.072	0.18	+0.069
surface toluene (ppbv)	0.17	+0.17	0.37	+0.066
surface xylene (ppbv)	0.12	+0.20	0.27	+0.071
surface isoprene (ppbv)	0.16	+0.20	0.29	+0.34
surface HCHO (ppbv)	0.72	+0.089	1.08	+0.012
surface CH_3CHO (ppbv)	0.33	+0.19	0.42	+0.34
surface PAN (ppbv)	0.32	+0.12	0.35	+0.004
surface CO (ppbv)	129	+0.007	155	+0.040
surface CO_2 (ppmv)	396.4	+0.0003	401.1	+0.003
surface SO_2 (ppbv)	0.21	+0.16	0.30	+0.49
surface daytime O_3 (ppbv)	39.5	+0.014	38.8	+0.010
surface O_3 (ppbv)	38.2	+0.0097	36.5	+0.028
surface H_2O (g) (ppmv)	9,850	−0.008	8,724	−0.041
column CH_4 (g/m^2)	9.47	+0.0072	9.47	+0.062
column C_2H_6(g/m^2)	0.0086	+0.64	0.0085	+5.0
column C_4H_6(g/m^2)	0.000006	+0.040	0.00003	+0.10
column C_6H_6(g/m^2)	0.0022	+0.0054	0.0019	+0.027
column toluene (g/m^2)	0.00073	+0.010	0.0011	+0.17
column xylene (g/m^2)	0.00033	+0.014	0.00064	+0.14
column isoprene (g/m^2)	0.00011	+0.087	0.00029	−0.021
column HCHO (g/m^2)	0.0016	+0.018	0.0021	+0.090
column CH_3CHO (g/m^2)	0.0015	+0.042	0.0015	+0.23
column PAN (g/m^2)	0.0056	+0.011	0.0058	+0.033
column CO (g/m^2)	0.90	−0.00004	0.86	+0.017
column SO_2 (g/m^2)	0.0014	+0.031	0.0017	+0.20
column O_3 (g/m^2)	7.40	+0.0003	6.25	+0.0015
column H_2O (kg/m^2)	11.8	−0.01	11.5	−0.051
surface total $PM_{2.5}$ ($\mu g/m^3$)	35.5	+0.11	31.8	+0.072
surface dry $PM_{2.5}$ ($\mu g/m^3$)	14.8	+0.037	20.6	+0.073
surface all-size BC ($\mu g/m^3$)	0.22	+0.42	0.70	+0.034

DOI: 10.1021/acs.est.9b01495
Environ. Sci. Technol. XXXX, XXX, XXX−XXX

Table 4. continued

species	California no leak	California leak minus no leak (percent change)	Los Angeles no leak	Los Angeles leak minus no leak (percent change)
surface all-size POM ($\mu g/m^3$)	1.20	+0.27	3.23	+0.063
surface all-size SOM ($\mu g/m^3$)	1.05	+0.22	1.11	+0.068
surface all-size H_2O (aq) ($\mu g/m^3$)	31.4	+0.094	15.3	+0.056
surface all-size S(VI) ($\mu g/m^3$)	1.07	−0.0081	0.99	+0.073
surface all-size NO_3^- ($\mu g/m^3$)	2.65	+0.19	5.33	+0.14
surface all-size NH_4^+ ($\mu g/m^3$)	0.69	+0.19	1.35	+0.080
surface all-size Na^+ ($\mu g/m^3$)	3.48	+0.021	2.70	+0.016
surface all-size soil dust ($\mu g/m^3$)	2.47	−0.13	8.08	+0.11
clear-sky 550 nm AOD	0.17	+0.027	0.16	−0.018
column aerosol number (no./cm^2)	2.8×10^9	−0.0092	4.3×10^9	+0.026
column dry aerosol mass (mg/m^2)	45.6	−0.031	44.1	−0.063
column BC (mg/m^2)	0.23	+0.065	0.51	+0.23
column POM (mg/m^2)	1.88	+0.064	2.72	+0.18
column SOM (mg/m^2)	2.19	+0.037	2.56	+0.21
column S (VI) (mg/m^2)	5.08	−0.0064	4.76	+0.026
column NO_3^- (mg/m^2)	4.08	+0.017	6.16	+0.023
column NH_4^+ (mg/m^2)	1.12	+0.00027	1.71	+0.0091
column aer-H_2O (aq) (mg/m^2)	31.2	−0.078	16.8	−0.005
column Na^+ (mg/m^2)	6.32	+0.013	4.75	+0.007
column soil dust (mg/m^2)	14.5	−0.13	11.8	−0.42
O_3 8 h mortalities during simulation[c]	179	+0.095	61	+1.0
$PM_{2.5}$ mortalities during simulation[d]	9,008	+0.35	3,689	−0.14

[a]All simulations started October 23, 2015, 0600 GMT. The California simulation ended March 3, 2016, 1800 GMT (132.5 days). The Los Angeles simulation ended January 23, 2016, 1800 GMT (92.5 days). [b]Divide milligrams per square meter by 1.9637 to obtain Tg. TOA: top of the atmosphere (top of model, 47.3 hPa for both the California and Los Angeles domains). TIR: thermal infrared. UV: ultraviolet. TKE: turbulence kinetic energy. CCN: cloud condensation nuclei. IDN: ice deposition nuclei. AOD: aerosol optical depth. $PM_{2.5}$: particles below 2.5 μm in diameter. POM: primary organic matter. SOM: secondary organic matter. Surface values are at about 15 m above ground level. [c]Premature mortalities per year due to short-term ozone exposure over each model domain were obtained by summing estimated mortalities among all near-surface grid cells in the domain. Mortalities were calculated in each surface grid cell using the common health effects equation, provided in eq 1 of ref 13, which takes into account population, pollution concentration, an all-cause annual mortality rate, and a relative risk of mortality or morbidity per unit change in concentration. Population is distributed spatially in each domain based on data; pollutant concentrations are determined over time from the GATOR-GCMOM model, and all-cause mortalities and relative risks are summarized here. The all-cause mortality rate used throughout California was 819 mortalities per year per population of 100 000. Ideally, this would vary by county, but a single number was used. The high, medium, and low fractional increases in the number of premature mortalities from all causes due to ozone were taken as 0.006, 0.004, and 0.002, respectively, per 10 ppbv increase in daily 1 h maximum ozone.[31] These fractional increases were multiplied by 1.33 to convert the risk associated with a 10 ppbv increase in 1 h maximum O_3 to that associated with a 10 ppbv increase in 8 h average O_3.[13] It was assumed no health effects from ozone occurred under a threshold of 35 ppbv. The mortalities per year in each grid cell were multiplied by the fraction of one year that the simulation was run for and summed over all surface grid cells to give the mortalities during the simulation period. The table shows only the middle premature mortality estimate. [d]The mortality rate due to long-term $PM_{2.5}$ exposure was also calculated for each model surface grid cell from eq 1 of ref 13. However, for $PM_{2.5}$, this equation was applied to the all-cause death rate of those ≥30 years, 809.7 mortalities per year per population of 100 000.[13] Increased premature mortality risks to those ≥30 years were assumed to be 0.008 (high), 0.004 (medium), and 0.001 (low) per 1 $\mu g/m^3$ $PM_{2.5}$ for $PM_{2.5}$> 8 $\mu g/m^3$ (see ref 29). From 0 to 8 $\mu g/m^3$, the increased risks were assumed to be a quarter of the risks for those >8 $\mu g/m^3$ to account for reduced risk near zero $PM_{2.5}$. A more updated set of relative risks from ref 30 is 0.0076 (high), 0.0055 (medium), and 0.0035 (low), with a low threshold of 5.8 ug/m^3 and no relative risk below the threshold. The medium Krewski et al. relative risk gives premature mortalities 51% to 34% to 28% higher than does the medium Pope et al. relative risk for ambient $PM_{2.5}$ concentrations ranging from 8 to 35 $\mu g/m^3$ to 100 $\mu g/m^3$, respectively. The Krewski et al. risks were unfortunately not included during the simulations to compared results from using the Pope et al. data with, but rough estimates of the results using the Krewski et al. data set are provided in the text. The mortalities per year in each grid cell were multiplied by the fraction of 1 year that the simulation was run for and summed over all surface grid cells to give the mortalities during the simulation period. The table shows only the middle premature mortality estimate.

Wunch et al.[5] estimate 2010 ethane emissions as 13 Gg-C_2H_6/year and, thus, much closer to the overall background ethane emissions used here. The much more significant underestimate in the methane emissions in the NEI is likely due to underestimates in pipeline natural gas leaks and agricultural emissions in the NEI inventory, in comparison with the work of Wunch et al.[5] Because background emissions occur in both the baseline and perturbation simulation, they are not expected to affect the conclusions of this study.

3. SIMULATIONS

Two pairs of global-through-local nested simulations were performed. The domains for one pair were a global domain and a nested California domain, both defined in Table 1. The domains for the other pair included a global domain, a nested California domain, and an innermost nested Los Angeles domain (Table 1). The advantages of the California pair of simulations are that it covers a much larger area than does the Los Angeles pair and does not have any discontinuous boundary conditions within California; however, the California pair is at a coarser horizontal resolution, thus noisier than the Los Angeles pair.

DOI: 10.1021/acs.est.9b01495
Environ. Sci. Technol. XXXX, XXX, XXX−XXX

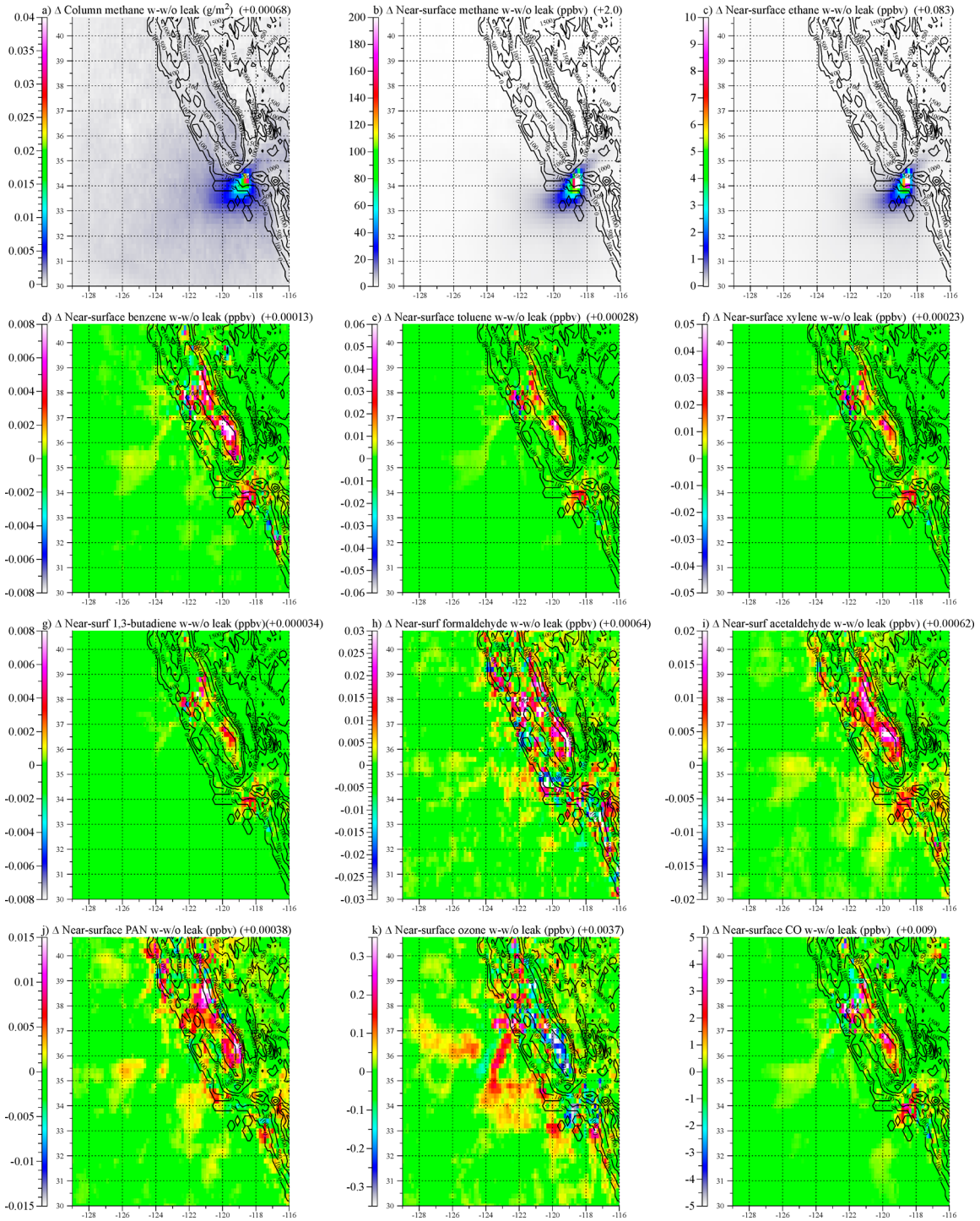

Figure 2. Simulation-averaged (from October 23, 2015 at 0600 GMT to March 3, 2016 at 1800 GMT, or 132.5 days) column or near-surface differences in results between the two California simulations (Table 1): one that included the Aliso Canyon leak and the other, which did not.

Vertically, the global domain had 68 σ-pressure layers from the ground to 0.219 hPa (~60 km), including 15 layers in the bottom 1 km and 500 m resolution from 1 to 21 km. All nested domains had 55 layers from the surface to 47.3 hPa, matching exactly the bottom 55 σ-pressure levels of the 68-layer global domain. Emissions entered all domains, and all gas, aerosol, radiative, dynamic, and surface processes were solved in all domains. Gases and particles were transported one way from the coarser to finer domains, allowing for the long-range transport of pollutants into finer domains. Clouds were not transported from coarser to finer domains, but the liquid and ice water from clouds in coarser domains were evaporated and transported to finer domains where the clouds could reform.

The California pair of simulations included one simulation with the Aliso Canyon leak occurring in the California domain and the other without. No leak occurred in the global domain in either simulation (thus the global calculations were exactly the same in both simulations). The reason for keeping the global domain constant was to eliminate deterministic chaotic variation entering the boundaries of the California domain.

DOI: 10.1021/acs.est.9b01495
Environ. Sci. Technol. XXXX, XXX, XXX−XXX

The California simulations ran for 132.5 days (from October 23, 2015 at 0600 GMT to March 3, 2016 at 1800 GMT).

The Los Angeles pair of simulations included one simulation with the Aliso Canyon leak occurring in the Los Angeles domain and the other without. No leak occurred in either the global or California domain in either simulation (thus, the global and California calculations were identical in both simulations). As such, perturbations occurred only in the Los Angeles domain due to the leak. The Los Angeles simulations ran for 92.5 days, from October 23, 2015 at 0600 GMT to January 23, 2016 at 1800 GMT.

Upon completion of each pair of simulations, differences from the innermost domain were taken to estimate the impacts on health, atmospheric composition, weather, and climate of the Aliso Canyon leak. Meteorological fields in all domains were initialized with Global Forecast System (GFS) 0.5° × 0.5° reanalysis fields[27] for October 23, 2015 at 0600 GMT. GFS fields are useful for initialization because they provide a consistent set of many meteorological parameters for the whole Earth.

4. RESULTS AND DISCUSSION

Figure 1 compares GATOR-GCMOM model results for some parameters during the first month of simulation for the California domain (defined in Table 1) with GFS reanalysis data from after the start of simulation.[27] GFS results were obtained by averaging individual GFS files four times per day each day over the same month-long period. Considering that GFS assimilates observations for each reanalysis field, whereas GATOR-GCMOM does not, the similarities in the spatial distribution of results are encouraging.

In 2015, CARB[28] measured near-surface methane hourly at five sites in California, all in the Central Valley. The closest site to Aliso Canyon was the Arvin-Di Giorgio site (35.23918 N, 118.78863 W), 104.8 km to the northwest of the Aliso Canyon leak. The next nearest site was over 300 km away from Aliso Canyon. The mean methane mixing ratios at the Arvin site from October 23, 2014 to February 11, 2015 and for the same periods in 2015−16 and 2016−17 were 2885, 2485, and 2450 ppbv, respectively. Thus, the mean mixing ratio during the full Aliso Canyon leak period (2015−16) was 13.9% lower than that during the same period the year before and 1.4% higher than that during the same period the year after. As such, the interannual variation of methane in the surface data at this site was larger than the perturbation (otherwise, the 2015−16 mean would be larger than the 2014−15 mean). If just the first 15 days of the leak are considered, the mean mixing ratio October 23, 2015 to November 6, 2015 is now only 6.1% lower than that during the same period the previous year and 1.9% higher than that during the same period the year after. Thus, the perturbation during the early phase of the leak is more detectable in the data but is still less than is the interannual variation. Similarly, the California model simulations here found that the average increase in near-surface methane at the Arvin site during the full leak period was only ∼3 ppbv and, during the first 15 days, only ∼7 ppbv.

Table 4 and Figures 2 and 3 show modeled differences with minus without the leak in the California domain from the nested California simulations. Table 4 and Figures 4 and 5 show differences in the Los Angeles domain from the nested Los Angeles simulations. Like from any plume source, emissions from Aliso Canyon increased the atmospheric near-surface mixing ratios and column loadings of multiple

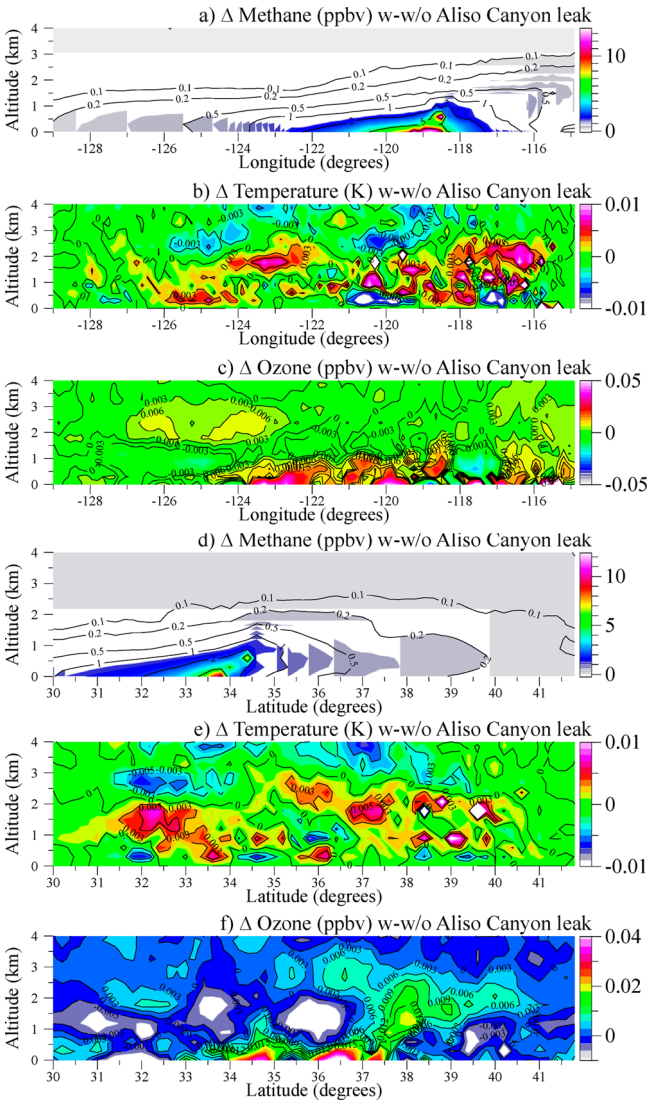

Figure 3. Same information as that given in Figure 2 but for time-averaged and either zonal (latitude−altitude) or meridianal (longitude−altitude) domain-averaged differences.

directly emitted hydrocarbons (e.g., methane, ethane, benzene, tolune, and xylene, among others listed in Table 2) that peaked in the vicinity of Aliso Canyon but spread in decreasing amounts throughout California, particularly the Los Angeles Basin, Central Valley, and San Francisco Bay Area (Figures 2 and 4). Figures 3 and 5 show that, in the simulation average, the methane plume spread not only horizontally throughout the entire California and Los Angeles domains but also vertically up to 3 km at appreciable levels.

Oxidation of the leaked hydrocabons increased near-surface and column carbon monoxide, formaldehyde, acetaldehyde, peroxyacetyl nitrate (PAN), and ozone, on average, in California and Los Angeles (Table 4 and Figures 2−5).

The increase in methane aloft increased temperatures aloft and more than at the surface (Figures 3 and 5), stabilizing the air in California and Los Angeles. The higher near-surface air temperatures due to the local emissions of methane are analogous to the higher near-surface air temperatures due to carbon dioxide domes over cities.[13] In the present case, the increase in methane slightly increased the top-of-the-model net downward thermal-infrared irradiance over both the California

DOI: 10.1021/acs.est.9b01495
Environ. Sci. Technol. XXXX, XXX, XXX−XXX

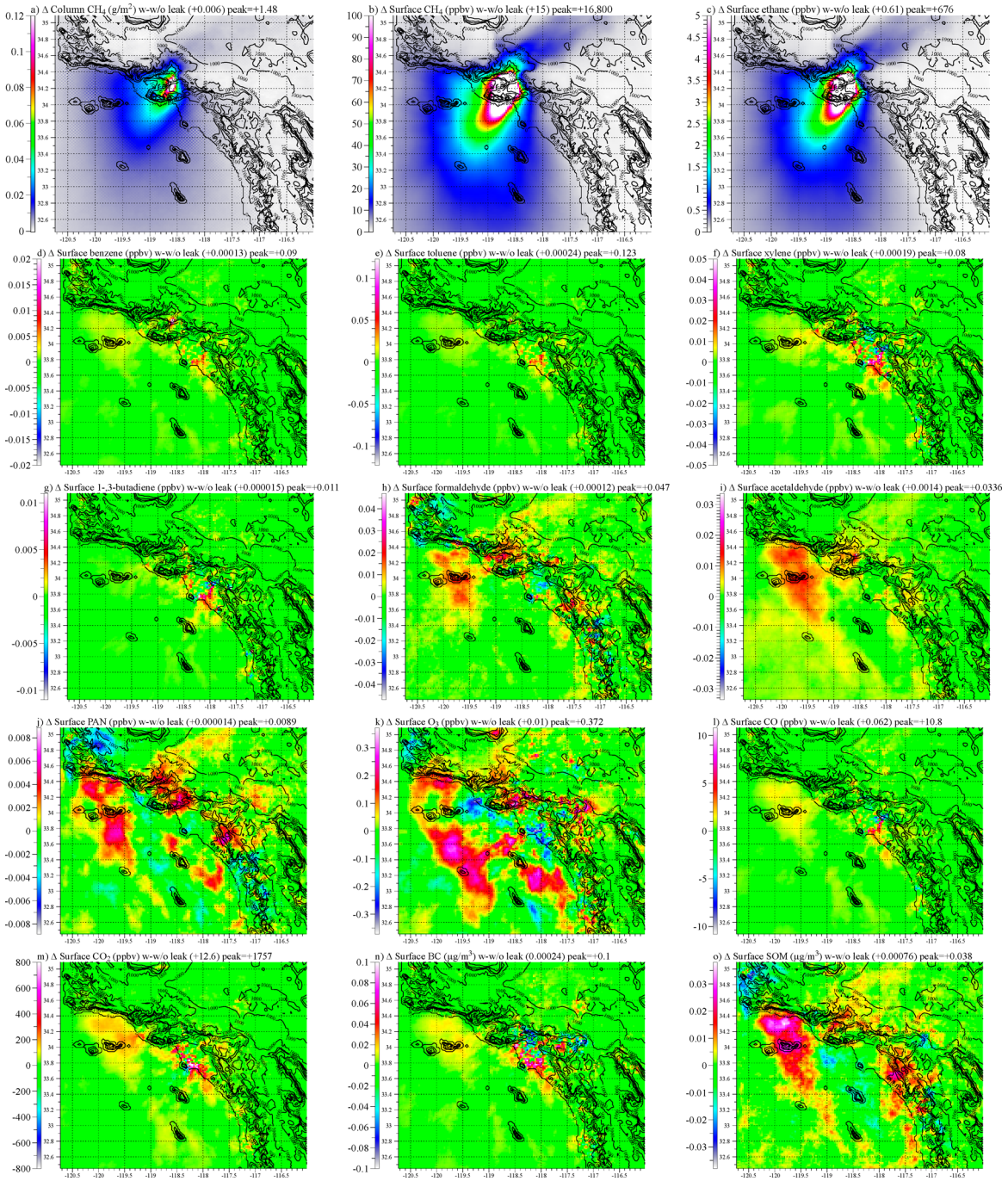

Figure 4. continued

DOI: 10.1021/acs.est.9b01495
Environ. Sci. Technol. XXXX, XXX, XXX−XXX

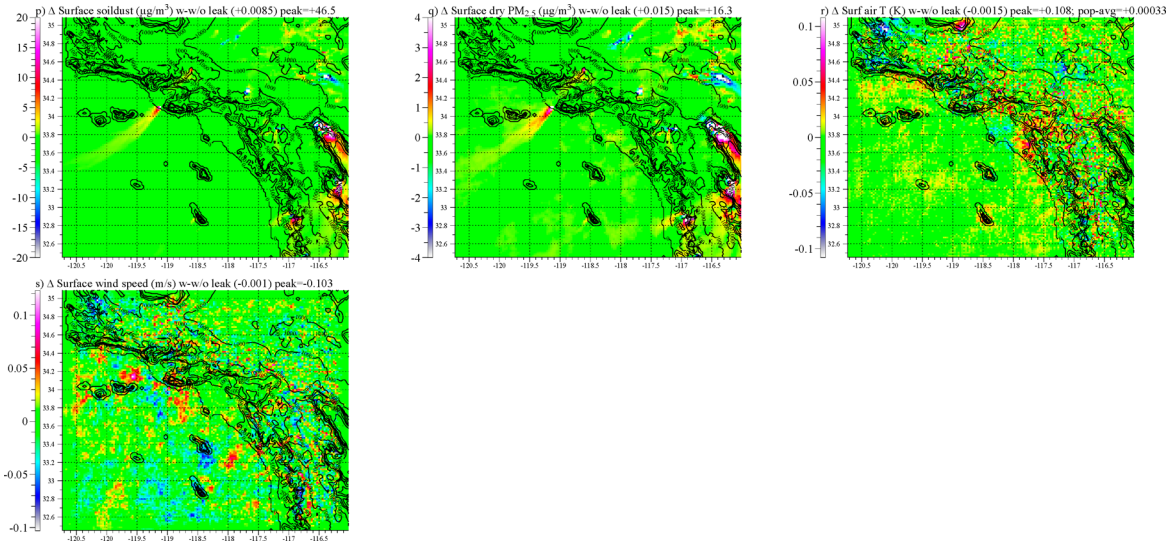

Figure 4. Simulation-averaged (from October 23, 2015 at 0600 GMT to January 23, 2016 at 1800 GMT, or 92.5 days) column or near-surface differences between the two Los Angeles simulations (Table 1): one that included the Aliso Canyon leak and the other, which did not.

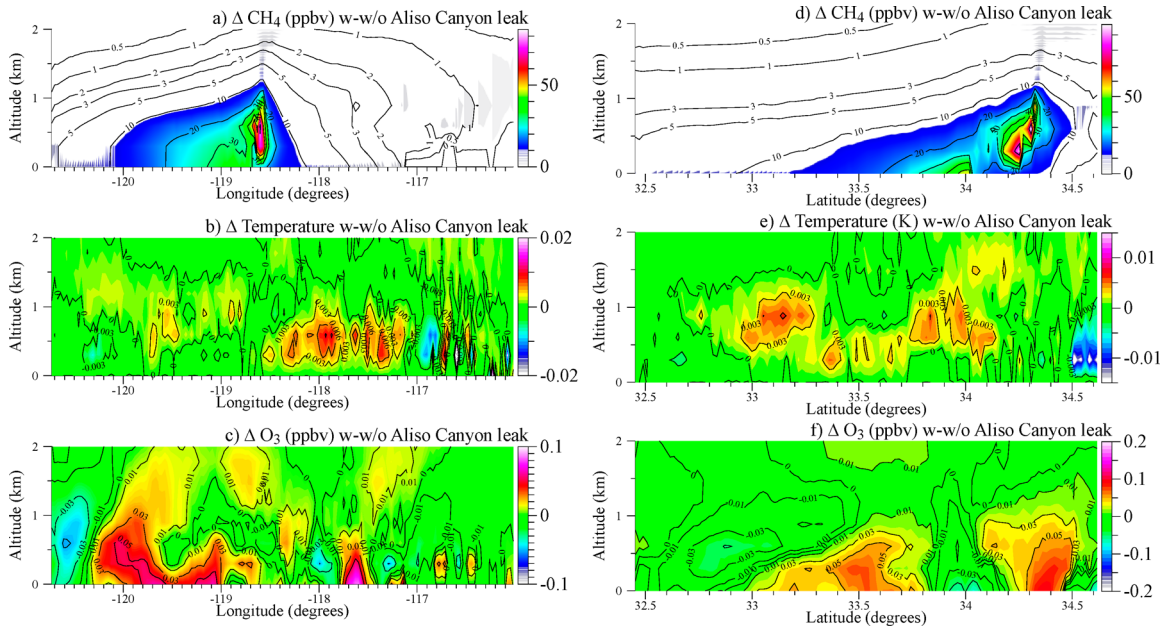

Figure 5. Same information as that for Figure 4 but for time-averaged and either zonal (latitude−altitude) or meridianal (longitude−altitude) domain-averaged differences.

and Los Angeles domains, creating a positive net radiative forcing due to the leak (Table 4).

Both higher temperatures aloft and more stable air aloft due to methane slightly reduced cloud fraction, cloud optical depth, and precipitation in California and Los Angeles but to a greater degree in Los Angeles (Table 4). The reduction in precipitation resulted in less rainout and washout of particles, increasing $PM_{2.5}$, on average, with a greater percentage increase in Los Angeles than in California as a whole (Table 4 and Figures 3 and 5). Thus, not only did the Aliso leak increase the chemical formation of secondary gas air pollutants, such as ozone, but also, it reduced the wet deposition of particles, generally increasing their surface and column concentrations. Over both the California and Los Angeles domains, the average surface and column concentrations of black carbon, primary and secondary organic carbon, sulfate, nitrate, and ammonium increased slightly due to the leak (Table 4).

The increase in the concentrations of both scattering and absorbing particles due to the reduction in precipitation caused by the leak stabilized the air further, reducing near-surface wind speed and precipitation more in a positive feedback loop, as expected from previous work.[16] The wind speed reduction was greater in Los Angeles than over California as a whole, whereas absorbing aerosol components warm the air relative to the ground, both absorbing and scattering aerosol components reduce radiation to the ground, cooling the ground relative to the air. Both factors stabilize the air, and stabilizing the air reduces the vertical transfer of horizontal momentum from aloft to the surface, slowing near-surface wind speeds.[16] The stagnation in both wind speed and precipitation increased the concentrations of aerosol components aside from wind-driven

DOI: 10.1021/acs.est.9b01495
Environ. Sci. Technol. XXXX, XXX, XXX−XXX

soil dust, whose column concentration decreased slightly due to the slight reduction in wind speed in locations of loose soil dust (Table 4 and Figure 4).

The main components of air pollution health problems are ozone, particles smaller than 2.5 μm in diameter ($PM_{2.5}$), and carcinogens (primarily formaldehyde, acetaldehyde, 1,3-butadiene, and benzene). The footnote to Table 4 describes how premature mortalities due to each of these pollutant classes were calculated during each simulation. Table 4 indicates that the Aliso Canyon leak resulted in an estimated increase in premature ozone and $PM_{2.5}$ mortalities over the California domain. However, enhanced $PM_{2.5}$ due to the leak dominated health effects, causing an estimated +32 (9 to 54) additional premature mortalities throughout California during the simulation period compared with no leak. This represents an increase of about 0.35% over the modeled premature mortality rate due to background air pollution in the state during this period (Table 4). The number of premature mortalities in the Los Angeles basin from the California domain simulation was +11. Most of the rest of the premature mortalities were in the Central Valley and the San Francisco Bay Area. These numbers were derived using the relative risks observed by Pope et al.[29] However, the more recent Krewski et al.[30] relative risks raise the additional premature mortalities in California to an estimated +43 (15 to 66) and in Los Angeles to a mean of +15.

The number of mortalities due to enhanced ozone in the California domain was small (<1) (Table 4). This study does not examine the possible number of cancers resulting to workers attempting to contain the leak or residents living near the plume because the spatial resolution of the simulations was not high enough to estimate that.

Over the Los Angeles domain from the Los Angeles simulation, ozone mortalities also increased by <1. However, modeled $PM_{2.5}$ mortalities decreased by ∼−5 despite the fact that the Aliso leak resulted in near-surface $PM_{2.5}$ (Table 4 and Figure 4) increasing on average over the Los Angeles domain. This contradictory result is due to the fact that some decreases in soil dust $PM_{2.5}$ occurred by chance in locations of higher population than where other $PM_{2.5}$ components increased (e.g., Figure 5). This artifact would likely disappear over longer simulations, as in the longer California simulations, where $PM_{2.5}$ premature mortality increased. Because $PM_{2.5}$ premature mortalities depend heavily on changes in concentrations over populated areas, and particle concentrations usually vary significantly over short distances, small changes in the location of particles can have a relatively large impact on premature mortality calculations. Another difference between the Los Angeles and California simulations is that, although the Los Angeles domain had higher resolution than did the California domain, the Los Angeles domain had discontinuous boundaries near the Los Angeles Basin, where California domain meteorological and chemical values fed in. The California domain had no such discontinuous boundaries near Los Angeles, but it was at coarser resolution.

Applying the Krewski et al.[30] instead of the Pope et al.[29] mean relative risk gives an estimated reduction in $PM_{2.5}$ premature mortalities in the basin from this simulation as −7. However, combining this result with that for the Los Angeles Basin from the California domain gives a range of mean premature mortalities in the Los Angeles Basin from Aliso Canyon as −7 to +15.

In summary, the model results suggest that the Aliso Canyon leak may have increased the mixing ratios of emitted hydrocarbon gases throughout California. Atmospheric photochemical reactions increased the mixing ratios of carbon monoxide, formaldehyde, acetaldehyde, peroxyacetyl nitrate (PAN), and ozone. Increases in air temperatures aloft and lesser increases at the surface due to thermal-infrared absorption by methane stabilized the air over much of California, slightly reducing cloud fraction, cloud optical depth, precipitation, and near-surface wind speed. The reduction in precipitation, in particular, increased concentrations of most particle components, except for wind-driven soil dust, whose concentrations decreased due to slower near-surface wind speeds caused by the leak. Higher particle concentrations increased estimated premature mortality due to particles in the California as a whole. Ozone premature mortality increased but only slightly.

Overall, the Aliso Canyon blowout appears to have altered California's short-term weather, climate, and gas and particle pollution levels, thereby damaging human health in the state. This result suggests that future gas blowouts of similar or larger magnitude will also have impacts on weather, climate, and health. However, the impacts will vary in magnitude with location due to different weather patterns, geography, and population distributions. For example, Ten Hoeve and Jacobson[22] found a vastly different impact of radionuclide emissions from the Fukushima Daiichi nuclear meltdown versus from a hypothetical meltdown of similar magnitude at the Diablo Canyon nuclear facility in California. The reasons were the difference in wind patterns, the difference in geography (ocean to the east of land versus to the west of land), and the difference in the location of the point sources relative to nearby population centers. Despite the uncertainty of impacts in the future, what appears certain is that additional blowouts will occur given the huge growth in worldwide natural gas production and storage.

AUTHOR INFORMATION

Corresponding Author

*E-mail: jacobson@stanford.edu. Phone: 650-723-6836.

Notes

The author declares no competing financial interest.

ACKNOWLEDGMENTS

This project received funding from the NASA SMD Earth Sciences Division, the National Science Foundation (grant no. AGS-1441062), the City of Los Angeles, and the Stanford Woods Institute for the Environment. It also received computer support from the NASA high-end computing center.

REFERENCES

(1) Conley, S.; Franco, G.; Faloona, I.; Blake, D. R.; Peischl, J.; Ryerson, T. B. *Science* **2016**, *351*, 1317−1320.

(2) CARB (California Air Resources Board). Determination of total methane emissions from the Aliso Canyon natural gas leak incident. https://www.arb.ca.gov/research/aliso_canyon/aliso_canyon_methane_emissions-arb_final.pdf (accessed August 10, 2018).

(3) Thompson, D. R.; Thorpe, A. K.; Frankenberg, C.; Green, R. O.; Duren, R.; Guanter, L.; Hollstein, A.; Middleton, E.; Ong, L.; Ungar, S. Space-based remote imaging spectroscopy of the Aliso Canyon CH_4 superemitter. *Geophys. Res. Lett.* **2016**, *43*, 6571−6578.

(4) Gourdji, S. M.; Yadav, V.; Karion, A.; Mueller, K. L.; Conley, S.; Ryerson, T.; Nehrkorn, T.; Kort, E. A. Reducing errors in aircraft

DOI: 10.1021/acs.est.9b01495
Environ. Sci. Technol. XXXX, XXX, XXX−XXX

atmospheric inversion estimates of point-source emissions: the Aliso Canyon natural gas leak as a natural tracer experiment. *Environ. Res. Lett.* **2018**, *13*, 045003.
(5) Wunch, D.; Toon, G. C.; Hedelius, J. K.; Vizenor, N.; Roehl, C. M.; Saad, K. M.; Blavier, J.-F. L.; Blake, D. R.; Wennberg, P. O. Quantifying the loss of processed natural gas within California's South Coast Air Basin using long-term measurements of ethane and methane. *Atmos. Chem. Phys.* **2016**, *16*, 14091−14105.
(6) Barrett, M. L. U.S. natural gas losses, late 1870s to early 1950s: A compilation and evaluation of numerical estimates. http://www.searchanddiscovery.com/abstracts/html/2018/ace2018/abstracts/2837104.html (accessed August 13, 2018).
(7) Sempra Energy. Form 10-Q, United States Securities and Exchange Commission. http://investor.sempra.com/static-files/d7fefdc2-e075-42c8-b003-94a497546cc3(accessed March 7, 2019).
(8) Jacobson, M. Z. GATOR-GCMM: A global through urban scale air pollution and weather forecast model. 1. Model design and treatment of subgrid soil, vegetation, roads, rooftops, water, sea ice, and snow. *J. Geophys. Res.* **2001**, *106*, 5385−5402.
(9) Jacobson, M. Z. GATOR-GCMM: 2. A study of day- and nighttime ozone layers aloft, ozone in national parks, and weather during the SARMAP Field Campaign. *J. Geophys. Res.* **2001**, *106*, 5403−5420.
(10) Jacobson, M. Z. Analysis of aerosol interactions with numerical techniques for solving coagulation, nucleation, condensation, dissolution, and reversible chemistry among multiple size distributions. *J. Geophys. Res.* **2002**, *107* (D19), 4366.
(11) Jacobson, M. Z. Development of mixed-phase clouds from multiple aerosol size distributions and the effect of the clouds on aerosol removal. *J. Geophys. Res.* **2003**, *108* (D8), 4245.
(12) Jacobson, M. Z. Studying ocean acidification with conservative, stable numerical schemes for nonequilibrium air-ocean exchange and ocean equilibrium chemistry. *J. Geophys. Res.* **2005**, *110*, D07302.
(13) Jacobson, M. Z. The enhancement of local air pollution by urban CO_2 domes. *Environ. Sci. Technol.* **2010**, *44*, 2497−2502.
(14) Jacobson, M. Z. Investigating cloud absorption effects: Global absorption properties of black carbon, tar balls, and soil dust in clouds and aerosols. *J. Geophys. Res.* **2012**, *117*, D06205.
(15) Jacobson, M. Z. Effects of biomass burning on climate, accounting for heat and moisture fluxes, black and brown carbon, and cloud absorption effects. *J. Geophys. Res.* **2014**, *119*, 8980−9002.
(16) Jacobson, M. Z.; Kaufman, Y. J. Wind reduction by aerosol particles. *Geophys. Res. Lett.* **2006**, *33*, L24814.
(17) Jacobson, M. Z.; Kaufman, Y. J.; Rudich, Y. Examining feedbacks of aerosols to urban climate with a model that treats 3-D clouds with aerosol inclusions. *J. Geophys. Res.* **2007**, *112*, D24205.
(18) Jacobson, M. Z.; Streets, D. G. The influence of future anthropogenic emissions on climate, natural emissions, and air quality. *J. Geophys. Res.* **2009**, *114*, D08118.
(19) Jacobson, M. Z.; Ten Hoeve, J. E. Effects of urban surfaces and white roofs on global and regional climate. *J. Clim.* **2012**, *25*, 1028−1044.
(20) Jacobson, M. Z.; Nghiem, S. V.; Sorichetta, A.; Whitney, N. *Ring of impact* from the mega-urbanization of Beijing between 2000 and 2009. *J. Geophys. Res.* **2015**, *120*, 5740−5756.
(21) Jacobson, M. Z.; Nghiem, S. V.; Sorichetta, A. Short-term impacts of the mega-urbanizations of New Delhi and Los Angeles between 2000 and 2009. *J. Geophys. Res.: Atmos.* **2018**, *124*, 35−56.
(22) Ten Hoeve, J. E.; Jacobson, M. Z. Worldwide health effects of the Fukushima Daiichi nuclear accident. *Energy Environ. Sci.* **2012**, *5*, 8743−8757.
(23) Toon, O. B.; McKay, C. P.; Ackerman, T. P.; Santhanam, K. Rapid calculation of radiative heating rates and photodissociation rates in inhomogeneous multiple scattering atmospheres. *J. Geophys. Res.* **1989**, *94*, 16287−16301.
(24) Clarke, L.; Edmonds, J.; Jacoby, H.; Pitcher, H.; Reilly, J.; Richels, R. Scenarios of Greenhouse Gas Emissions and Atmospheric Concentrations, *Sub-report 2.1A of Synthesis and Assessment Product 2.1 by the U.S. Climate Change Science Program and the Subcommittee on Global Change Research*; Department of Energy, Office of Biological & Environmental Research: Washington, DC, 2007.
(25) European Commission Joint Research Centre (JRC)/Netherlands Environmental Assessment Agency (PBL). Emission Database for Global Atmospheric Research (EDGAR). http://edgar.jrc.ec.europa.eu (accessed April 1, 2018).
(26) USEPA (United States Environmental Protection Agency). 2007/2008 Version 5 Air Emissions Modeling Platforms. https://www.epa.gov/air-emissions-modeling/20072008-version-5-air-emissions-modeling-platforms (accessed August 14, 2018).
(27) GFS (Global Forecast System). 0.5° × 0.5° Reanalysis Fields. https://www.ncdc.noaa.gov/data-access/model-data/model-datasets/global-forcast-system-gfs (accessed September 27, 2018).
(28) CARB (California Air Resources Board). Greenhouse gas data query tool. https://www.arb.ca.gov/aqmis2/res/aqdselect.php?tab=daily (accessed March 10, 2019).
(29) Pope, C. A., III; Burnett, R. T.; Thun, M. J.; Calle, E. E.; Krewski, D.; Ito, K.; Thurston, G. D. Lung cancer, cardiopulmonary mortality, and long-term exposure to fine particulate air pollution. *JAMA* **2002**, *287*, 1132−1141.
(30) Krewski, D.; Jerrett, M.; Burnett, R. T.; Ma, R.; Hughes, E.; Shi, Y.; Turner, M. C.; Arden Pope, C., III; Thurston, G.; Calle, E. E.; Thun, M. J. *Extended follow-up and spatial analysis of the American Cancer Society study linking particulate air pollution and mortality*; Health Effects Institute: Boston, MA, 2009.
(31) Ostro, B. D.; Tran, H.; Levy, J. I. The health benefits of reduced tropospheric ozone in California. *J. Air Waste Manage. Assoc.* **2006**, *56*, 1007−1021.

DOI: 10.1021/acs.est.9b01495
Environ. Sci. Technol. XXXX, XXX, XXX−XXX